Volume 18, Number 2, 2025. pp. 197-206

Jordan Journal of Physics

ARTICLE

Sensing Efficacy of ZnO Film Towards Ethanol and Acetone

Dinesh K. CHAUDHARY[a], **Surya K. JOSHI**[b] and **Agni DHAKAL**[c]

[a] *Physics Department, Amrit Campus, Tribhuvan University, Kathmandu, 44600 Nepal.*

[b] *Central Department of Chemistry, Tribhuvan University, Kirtipur, Kathmandu, 44618 Nepal.*

[c] *Research Division, Nepal Academy of Science and Technology, Khumaltar, Lalitpur, 44700, Nepal.*

Doi: **https://doi.org/10.47011/18.2.9**

Received on: 18/12/2023; *Accepted on: 28/03/2024*

Abstract: In this work, zinc oxide nanoparticles (ZnO NPs) were synthesized via the co-precipitation method and analyzed by X-ray diffraction (XRD), scanning electron microscopy (SEM), and energy dispersive X-ray diffraction (EDX). The ethanol and acetone vapor detection abilities of the ZnO film were comprehensively examined at temperatures ranging from 100°C to 330°C. The XRD results revealed a polycrystalline nature with a mean crystallite size of 27.3898 ± 0.5472 nm. The SEM and EDX analyses demonstrated the formation of nano-leaf structures of ZnO. Gas sensing measurements showed a higher response of 52.08 ± 1.23 and 25.62 ± 1.21 at 285 °C at 800 ppm ethanol and acetone vapor exposure, respectively, i.e., selectivity towards ethanol. The film exhibited rapid response times of 5 s for ethanol and 11 s for acetone. Repeatability and stability tests over multiple cycles demonstrated consistent performance, surpassing that of similar reported sensors. These results support the development of a cost-effective and efficient gas sensor capable of detecting ethanol and acetone vapors at concentrations as low as 40 ppm, which is below the permissible exposure limits set by the Occupational Safety and Health Administration (OSHA).

Keywords: Zinc Oxide, Gas response, Response time, Selectivity.
PACs Code: 07.07 Df.

1. Introduction

Over the past couple of decades, metal oxide semiconductor (MOS) nanomaterials have garnered significant attention due to their wide range of industrial uses, including biomedical, chemical, and food industries, as well as in optoelectronic devices, resonators, solar cells, agriculture, etc. [1–4]. Among various MOS, ZnO is emerging as a potential material because of its tunable electrical, optical, and surface characteristics, which are useful for a variety of applications, such as photocatalytic activity, solar cells, gas sensors, and so on [5–7]. One of the most notable uses of ZnO is as a gas-sensing material, because its sensing capability is well known and controlled mostly by its surface properties and working temperature [8–10]. ZnO responds to gas exposure. However, the lower response, high operating temperature, and selectivity are the major problems. Currently, significant efforts are underway to enhance the gas-sensing capabilities and selectivity of MOS-based sensors through surface modification, metal doping, conducting polymer doping, nano-composing, etc. [8, 11–14]. Among these strategies, surface modification has been shown to be effective in improving gas sensing capabilities [8, 9]. The morphology of ZnO depends strongly on the preparation method [15–18]. In this regard, the co-precipitation method has proven to be one of the most essential, low-

Corresponding Author: Dinesh Kumar CHAUDHARY **Email**: dinesh.chaudhary@ac.tu.edu.np

cost, and time-consuming approaches for producing ZnO nanoparticles. This method does not require a vacuum system and can yield substantial quantities in a single batch.

Acetone is a clear, colorless, volatile organic liquid that evaporates quickly. It is used as the laboratory solvent for materials like paints, grease, plastics, synthetic fibers, etc., and for rinsing glassware and equipment. Excessive exposure to acetone fumes can cause irritation of the eyes, nose, throat, and lungs in a couple of minutes. It can cause headaches, dizziness, damage to the nervous system, confusion, or unconsciousness [19–21]. Likewise, ethanol is a widely used toxic chemical in various industries, such as the production of food additives, medicines, antibacterial products, alcoholic drinks, and cosmetic products [22–24]. Its excessive exposure might have negative consequences for living beings. Exposure to ethanol vapor induces a ventricular and septal wall stiffening during growth [22, 25].

As a consequence of the above-mentioned things, there is a pressing demand for acetone and ethanol sensors capable of detecting low concentrations of vapor with fast and high response. ZnO film was found to be sensitive to both ethanol and acetone at the working temperature >300 ºC [24, 26-30]. However, reports focusing on the selectivity of ZnO among ethanol and acetone are scarce.

In this work, ZnO NPs were synthesized by the economical co-precipitation method and characterized to study their sensing capability towards ethanol and acetone vapors. The results of extensive investigations on the structural, morphological, and gas-sensing characteristics are presented and compared to the results of the published reports. This work reports a higher response of the 0.5 M ZnO film towards ethanol than towards acetone. Also, the gas response of 0.5 M ZnO film towards the investigated vapors (ethanol and acetone) was found to be higher at relatively lower operating temperatures than the available published reports [15, 17, 18, 20-22, 27, 28, 30]. In addition, the gas sensing mechanism of ZnO film is discussed.

2. Experimental

2.1 Materials

Analytical-grade chemicals [zinc acetate di-hydrate ($Zn(CH_3CO_2)_2{:}2H_2O$), ethanol (CH_3CH_2OH), sodium hydroxide (NaOH), stannous chloride di-hydrate ($SnCl_2{:}2H_2O$), conc. hydrochloric acid (HCl), deionized water, and vinegar] were used without further modifications throughout the experiment to synthesize ZnO NPs.

2.2 Preparation and Characterization

Clean glass substrates were initially coated with fluorine-doped tin oxide (FTO) layers via the spray pyrolysis technique. To make the FTO solution, 21.051 g of $SnCl_2{:}\ 2H_2O$ was dissolved in 10 ml concentrated hydrochloric acid using a magnetic stirrer at 90 ± 10 °C. After that, 40 ml of deionized water was added, and the mixture was stirred for 15 minutes at 60 ± 10 °C. Meanwhile, NH_4F was dissolved in 50 ml of deionized water in another vessel. Following that, both of these solutions were put together, stirred for 1 hour, and then aged for 24 hours [31].

For ZnO NPs synthesis, zinc acetate dihydrate was dissolved in ethanol and shaken using a magnetic stirrer for 2 hours at 60 ± 10°C. 2M NaOH solution was added dropwise to the solution under continual stirring conditions to form the precipitate (ppt), maintaining the PH 12 of the solution. The precipitated material was centrifuged at 2000 rpm, carefully scrubbed, and rinsed 5 times with deionized water. The obtained material was subsequently dried for 16 hours at 100°C in a furnace. The ZnO paste was made with ethanol and 3 drops of vinegar. The vinegar serves as a binder. The ZnO film was created on the FTO-coated glass substrate by spreading the paste using a sharp blade. The film was then annealed for 1 hour at 550 ± 2 °C and aged for an additional 21 days to adhere to the substrate [32]. Finally, the ZnO nanoparticles were analyzed using XRD, SEM, and EDX.

Gas-sensing performance was evaluated at 100–350 °C using a custom-built gas-detection system consisting of an airtight glass chamber with inlet and outlet ports. The chamber was placed on a digital temperature-controlled hot plate (TALBOYS 7X7 CER HP 230 V ADV, Henry Troemner, LLC, USA). The ZnO film was positioned inside the chamber facing downward. A Ni-Cr micro-heater allowed heating up to 370 °C, with temperature regulated via a variable-voltage power supply. To prevent condensation, the chamber temperature was maintained just above the boiling point of the test vapors.

The gas response or sensitivity of the device fabricated with the ZnO film was estimated by measuring the resistance of the ZnO film in two distinct environments: in air and in gaseous environments. The gas response (R) is defined as

$$R = \frac{R_a}{R_g} \quad (1)$$

Here, R_a and R_g are the ZnO film resistances in air and gaseous environments [28]. To measure the resistance, two electrodes were fabricated on the ZnO film using silver paste and copper wire. The electrodes were separated by 1 cm. The electrodes were connected to the ohm meter (multi-meter, Fluke 101) to measure the resistance of the ZnO film.

3. Results and Discussion

3.1 Structural analysis

The structural characteristics were examined using the X-ray diffraction (XRD) technique. Fig. 1 depicts the X-ray diffraction pattern of ZnO NPs, which was performed using an X-ray diffractometer (Bruker AXS D2 PHASER A26-X1-A2BOB2A-, Serial No: 207047) employing Cu-K radiation of wavelength 1.54056 Å. The existence of several prominent steep peaks in the XRD spectrum demonstrates the polycrystalline structure of ZnO. The prominent steep peaks observed at 2θ = 31.9763°, 34.6344°, 36.4623°, 47.7476°, 56.8084°, 63.0683°, 66.5568°, 68.1557°, 69.2983°, and 77.1542 ° corresponding to (100), (002), (101), (102), (110), (103), (200), (112), (201), and (202) planes, respectively, which have been found to be matching the normal range values of JCPDS card number 36-1451 [33]. There was no further impurity peaks observed, indicating that pure ZnO had been synthesized. The size of crystallites (D) was calculated using the Debye–Scherrer equation:

$$D = \frac{0.9\lambda}{\beta cos\theta} \quad (2)$$

Here, λ is the wavelength of X-radiation and β is the full width at half maximum of the diffraction peak.

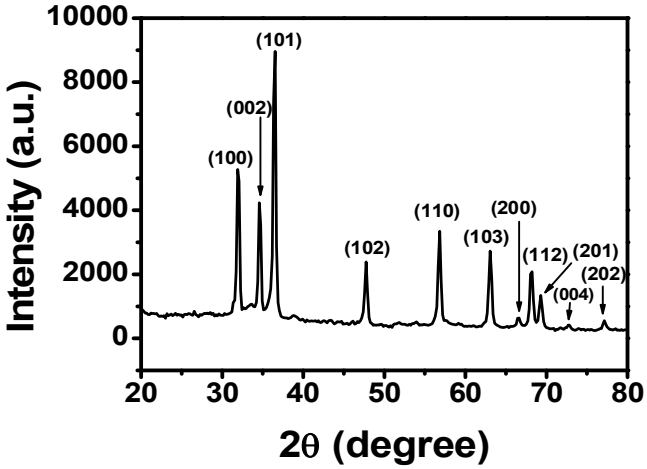

FIG. 1. XRD pattern of ZnO.

The crystallite size D and d-spacing corresponding to the most intense peak (101) were 28.4172 ± 0.9012 nm and 2.46123 ± 0.12011 Å, respectively. The mean crystallite was estimated to be 27.39 ± 0.5472 nm. The two lattice parameters, a and c, were estimated using formulas:

$$a = \frac{\lambda}{\sqrt{3}\, sin\theta} \quad (3)$$

and

$$c = \frac{\lambda}{sin\theta} \quad (4)$$

respectively [34, 35]. The values of a and c were 3.2280 ± 0.1199 Å and 5.1736 ± 0.0008 Å, respectively, with c/a = 1.5999 ± 0.0595, suggesting a hexagonal wurtzite phase.

3.2 Surface Morphology and Elemental Analysis

The gas-sensing characteristics of ZnO films depend critically on their surface morphology [8, 9]. The surface morphology was examined using a scanning electron microscope (SEM) and is depicted in Fig. 2(a). It clearly shows the nanoflake-like structure. The elemental composition was examined using the EDX technique, and the result is presented in Fig. 2(b). The EDX spectrum showed the atomic percentages of Zn and O as 48.03 and 51.97%, respectively, indicating the purity of the product.

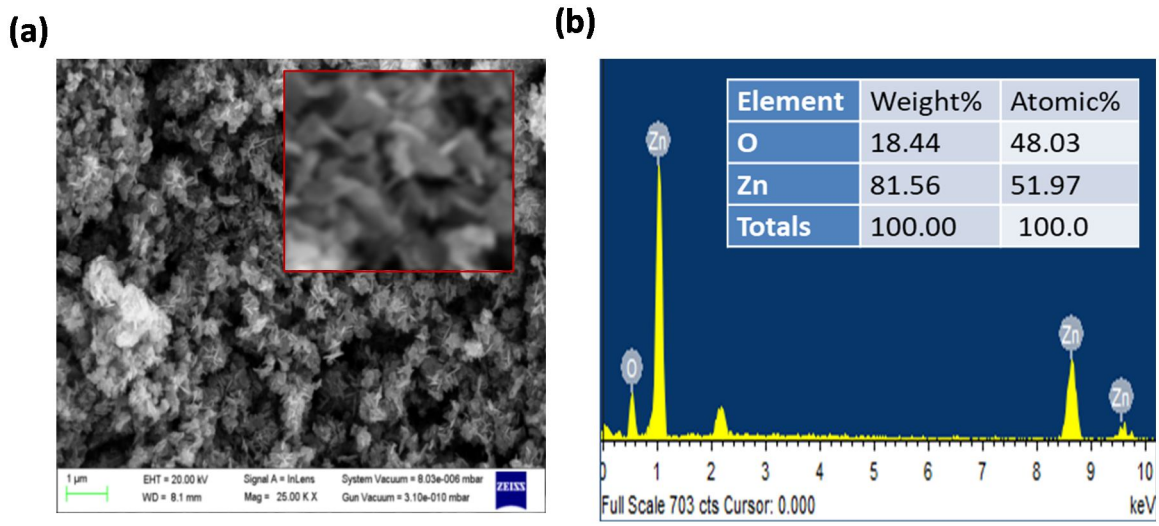

FIG. 2. (a) SEM image and (b) EDX spectra of ZnO.

3.3 Gas Sensing Behavior

The gas-sensing capability of ZnO-based gas sensors depends greatly on the temperature [36]. Initially, the gas-sensing capability was investigated over a temperature range of 100°C - 330°C at 800 ppm of ethanol and acetone exposure, separately. It was done by measuring the résistances R_a and R_g of the ZnO film in air and gaseous environments, respectively, and then calculating the gas response (R) using the formula in Eq. (1).

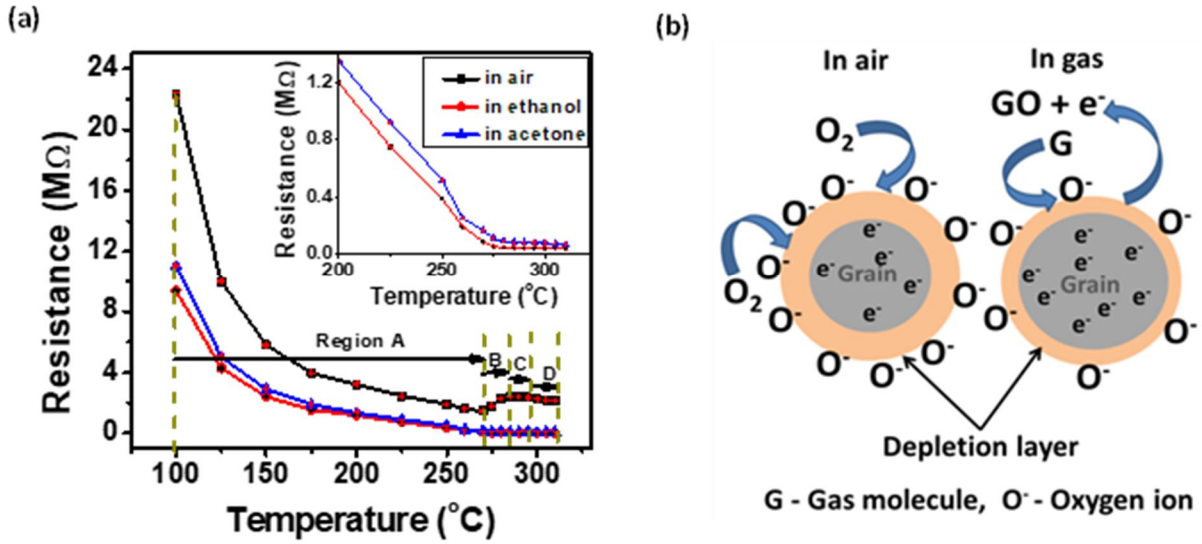

FIG. 3. (a) Resistance variation of the ZnO film with temperature in air, 800 ppm of ethanol and acetone vapors, (b) Illustration of gas-sensing mechanism of the ZnO film.

Figure 3(a) depicts the plot of resistance with temperature of the ZnO film in air, ethanol, and acetone vapor. The resistance of the ZnO film decreased with increasing température, exhibiting semiconducting behavior. To explain the variation of resistance of ZnO in air with temperature, the curve may be divided into four regions: A, B, C, and D. In région A, the resistance decreased with increasing temperature up to 270°C due to the thermal activation of conduction band électrons, which is the dominant factor. The resistance then increased with temperature rising to 285°C in region B, indicating the semiconducting characteristics. This increase is likely due to the formation of oxygen vacancies, which promotes the adsorption of oxygen molecules onto the ZnO surface [37]. The adsorbed oxygen captures free electrons from the conduction band, forming negatively charged oxygen species, thereby increasing the resistance of the film.

In region C (285–295 °C), the resistance remains nearly constant. This plateau suggests a dynamic equilibrium between the thermal

excitation of charge carriers and the oxygen adsorption process [38].

The resistance of the ZnO film decreased beyond 295 °C in region D, likely due to the dominant thermal activation of the electrons and desorption of oxygen species. The temperature around 285-295 °C is thought to be suitable for sensor functioning due to the small temperature dependence. [38].

The resistance of the sample was lower in a gaseous environment than in the air, as shown in Fig. 3(a). Also, the resistance of the sample was lower in ethanol than in acetone vapor [inset of Fig. 3(a)]. The classical model of gas-sensing can be used to explain it [Fig. 3(b)]. In the ambient atmosphere, the oxygen was adsorbed onto the ZnO surface, which extracted the electrons from the conduction band, and oxygen ions (O^-, O_2^-, or O^{2-}) were formed. It increased the depletion layer and the ZnO film resistance, as shown in Fig. 3(b) [39]. The form of adsorbed oxygen ions depends on the ZnO surface temperature. The oxygen adsorption and oxygen ion formation processes on the ZnO surface are expressed by Eqs. (5)-(8). At a temperature of 25–150 °C, O_2^- is the predominant species among the adsorbed oxygen ions, which indicates that oxygen ions are primarily adsorbed in the form of O_2^- ions at lower temperatures. As the temperature increases between 150 and 350 °C, the O_2^- ions decompose, and the adsorbed species consist of O^- and O^{2-} ions. Among these two species, the O^- ions become dominant. Finally, when the temperature surpasses 350 °C, O^{2-} ions become more prevalent on the ZnO surface [40].

$$O_{2(g)} \leftrightarrow O_{2(ads)} \quad (5)$$

$$O_{2(ads)} + e^- \leftrightarrow O_{2(ads)}^- \text{ (Room temperature to 150 °C)} \quad (6)$$

$$O_{2(ads)}^- + e^- \leftrightarrow 2O_{(ads)}^- \ (150 - 350\ ^\circ\text{C}) \quad (7)$$

$$O_{(ads)}^- + e^- \leftrightarrow O_{(ads)}^{2-} \text{ (above 350 °C)} \quad (8)$$

In the gaseous environment, the gas molecules interacted with oxygen ions and released the electrons back to the ZnO surface, which decreased the depletion layer and the resistance of ZnO [Fig. 4(b)]. The possible interaction of gas molecules with the oxygen ions and the release of electrons back to the ZnO surface are illustrated in Eqs. (9) and (10), respectively [27, 39].

$$CH_3CH_2OH(ethanol) + 6O_{ads}^- \rightarrow 2CO_2 + H_2O + 6e^- \quad (9)$$

$$CH_3COCH_3(Acetone) + 8O_{ads}^- \rightarrow 3CO_2 + H_2O + 8e^- \quad (10)$$

The resistance of the film decreased more in the case of ethanol exposure than in the case of acetone exposure [Inset of Fig. 4(a)]. It is attributed to the lower ignition point (365 °C) and smaller kinetic diameter (0.45 Å) of the ethanol molecule compared to that of acetone. The ignition point and kinetic diameter of acetone are 465 °C and 0.46 Å, respectively. The lower ignition point and smaller kinetic diameter of ethanol facilitate greater thermal activation and deeper penetration of ethanol vapor molecules into the porous structure of the ZnO film compared to acetone vapor molecules. This enables the ethanol molecules to interact more readily with a larger number of oxygen ions. Consequently, more electrons are released back to the ZnO surface, resulting in a greater reduction in resistance under ethanol exposure than under acetone exposure [40].

Figure 4 illustrates the relationship between gas response and temperature, measured separately at 800 ppm ethanol and acetone exposure. The gas response initially increased with rising temperature, reaching maximum values of 53.5284 ± 1.2311 for ethanol and 25.6119 ± 1.2311 for acetone, respectively, at 285 °C, and then decreased beyond this temperature. This behavior is due to the proportional relationship between gas response and the reaction rate coefficient K_{Eth} [40]. The reaction rate coefficient varies with temperature in Kelvin as:

$$K_{Eth}(T) = A\, e^{-E_a/k_B T} \quad (11)$$

where k_B is the Boltzmann constant, and E_a is the activation energy barrier of reaction [39].

As the temperature increases, thermal energy also increases. When the thermal energy approaches to E_a, the concentration of charge carriers increases significantly, enhancing oxygen adsorption onto the ZnO surface and resulting in a high sensor response. Beyond this temperature, oxygen desorption dominates, leading to a decrease in gas response [42].

The gas response of the ZnO film was higher under ethanol exposure than under acetone exposure. At 285 °C, the film exhibited gas responses of 53.5284 ± 1.2311 and 25.6119 ±

1.2311 to 800 ppm ethanol and acetone, respectively. This is attributed to the greater reduction in resistance upon ethanol exposure compared to acetone exposure [inset of Fig. 3(a)].

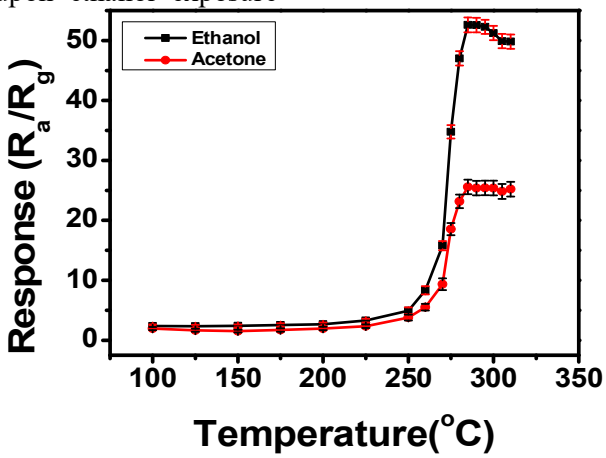

FIG. 4. Gas response variation with temperature at 800 ppm of ethanol and acetone exposure.

Further, the experiment was performed to study the repeatability and the capability of detecting low ppm of the targeted vapors. Figs. 5(a) and 5(b) illustrate the transient resistance responses at 800 ppm exposure of ethanol and acetone vapors, respectively, over four cycles at 285 °C. The resistance dropped to nearly the same stable value. The resistance dropped from an average value of 2.4612 ± 0.0039 MΩ to 0.0460 ± 0.0004 MΩ with an average gas response of 53.3222 ± 1.2311 under ethanol exposure and 2.2218 ± 0.0022 MΩ to 0.086 ± 0.0008 MΩ with an average gas response of 25.6235 ± 0.9735 under acetone exposure, respectively, indicating good repeatability.

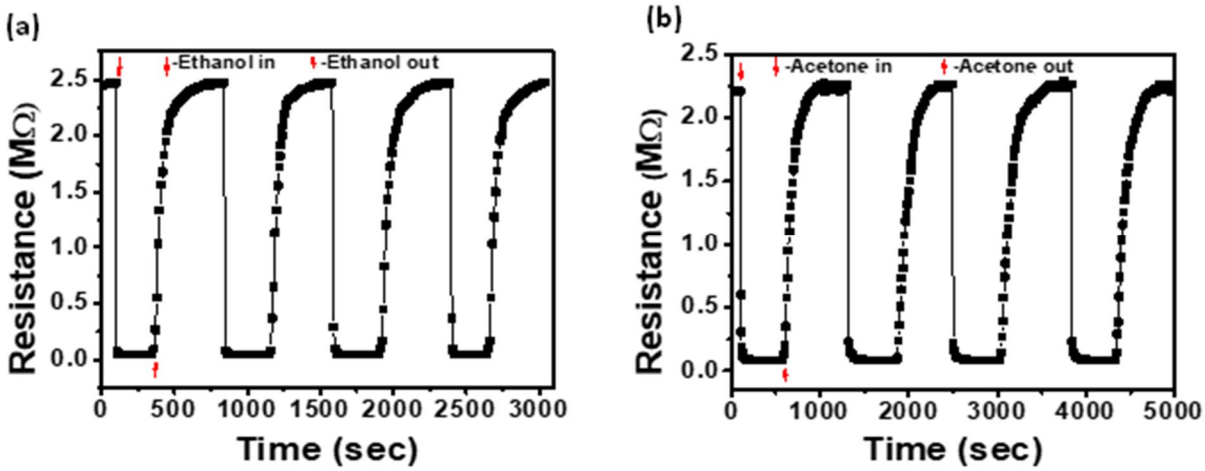

FIG. 5. Transient resistance response of the ZnO film at an exposure of 800 ppm of (a) ethanol, and (b) acetone vapors for four cycles.

Figures 6(a) and 6(b) show the plots of the transient resistance responses measured at 40–800 ppm ethanol and acetone exposure, respectively, at 285 °C. The resistance decreased abruptly at first and then acquired a stable value in both ethanol and acetone vapor environments. The resistance change was more significant at an exposure to higher amount of vapor. The average resistance of the ZnO NPs film changed from 2.4612 ± 0.0039 MΩ to 0.6333 ± 0.0057 MΩ at 40 ppm of ethanol exposure and 2.2218 ±0.0022 MΩ to 0.7351 ± 0.0066 MΩ at the same amount of acetone exposure.

Figure 7 shows the gas response of the ZnO film at various concentrations (40–800 ppm) of ethanol and acetone exposures. The film detected as low as 40 ppm of both vapors, with responses of 4.0618 ± 0.4923 for ethanol and 3.4912 ± 0.5813 for acetone. The gas response value was large at higher concentrations of vapor. This behavior is attributed to the greater surface coverage of the ZnO film by the test gas molecules at higher concentrations, which

enhanced their interaction with the adsorbed oxygen ions. The two essential gas sensing parameters are the response time and the recovery time. These refer to the times required for the resistance to change by 90% from the stable value following the exposure to, and removal of, the test gas from the sensing chamber, respectively.

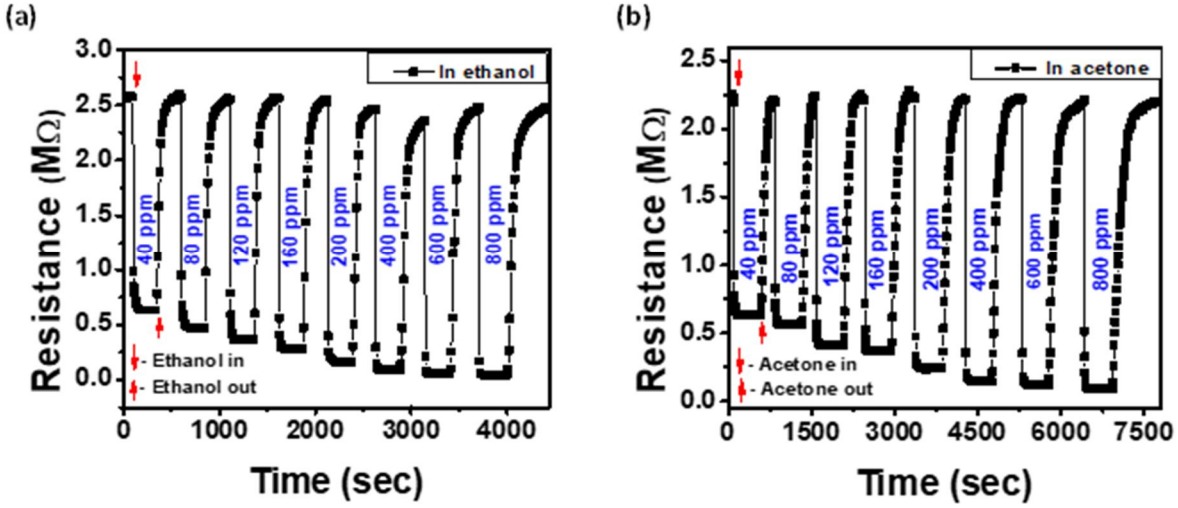

FIG. 6. Transient resistance responses of the ZnO nps film at an exposure of various concentrations (40-800 ppm) of (a) ethanol and (b) acetone vapors at 285 °C.

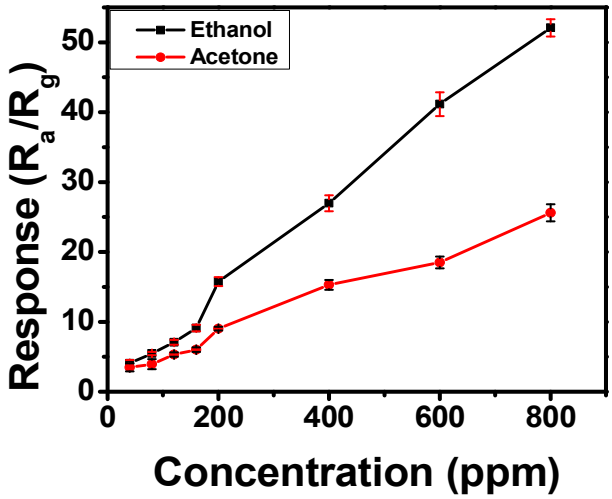

FIG. 7. Gas response at exposure various concentrations of ethanol and acetone

Figures 8(a) and 8(b) illustrate the graphical method of calculation of these two parameters at 800 ppm ethanol and acetone exposure at 285 °C. The plots of the response and recovery times with various concentrations (40-800 ppm) of tested vapors are depicted in Figs. 9(a)-9(b). The ZnO film exhibited a fast response and recovery in the case of ethanol exposure, with response times of 4.7 ± 0.3 to 6.1 ± 0.2 s and recovery times of 80.0 ± 0.7 to 148 ± 3.4 s for various concentrations. In contrast, for acetone exposure, the response and recovery times ranged from 9.4 ± 0.3 to 11.0 ± 0.3 s and 141.0 ± 0.7 to 290.7 ± 3.9 s, respectively. It may be due to the lower ignition point of ethanol than that of acetone, which facilitates the higher thermal activation and rapid ejection of ethanol vapor from the test chamber. As a result, the adsorption of oxygen started quickly.

The gas sensing results indicate that the gas sensing capability of the ZnO film was better for ethanol detection in comparison to acetone detection. The results of this study were compared with those of previously published studies (Tables 1 and 2). Compared to ZnO films made using other techniques, such as electrospinning [17], solvothermal [18], thermal evaporation [28], and RF magnetron sputtering [38], the 0.5 M ZnO film produced in our work showed improved gas sensing capability towards ethanol (Table 1). In addition, it demonstrated superior acetone sensing capability compared to other sensors made using other methods,

including the solvothermal and vapor-solid approaches [15, 18]. Furthermore, the relative analysis indicates that the ZnO film sensor operating temperature in this study was slightly lower than that of the published reports for detecting acetone (Table 2). Based on these findings, we conclude that the 0.5 M ZnO film can be effectively utilized as a sensing element for detecting both acetone and ethanol, with a notable selectivity towards ethanol.

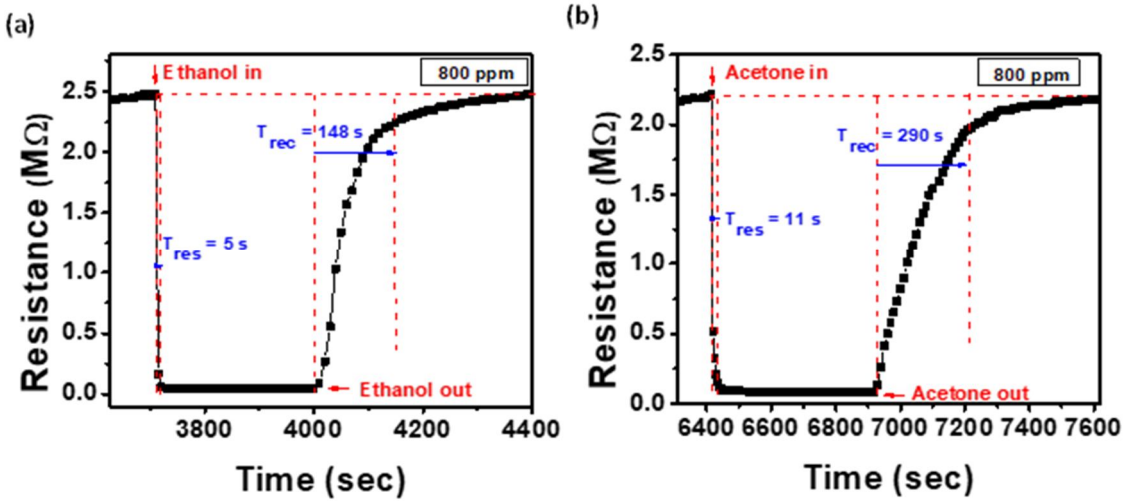

FIG. 8. Graphical calculation of response time and recovery time at 800 ppm (a) ethanol and (b) acetone vapors exposure.

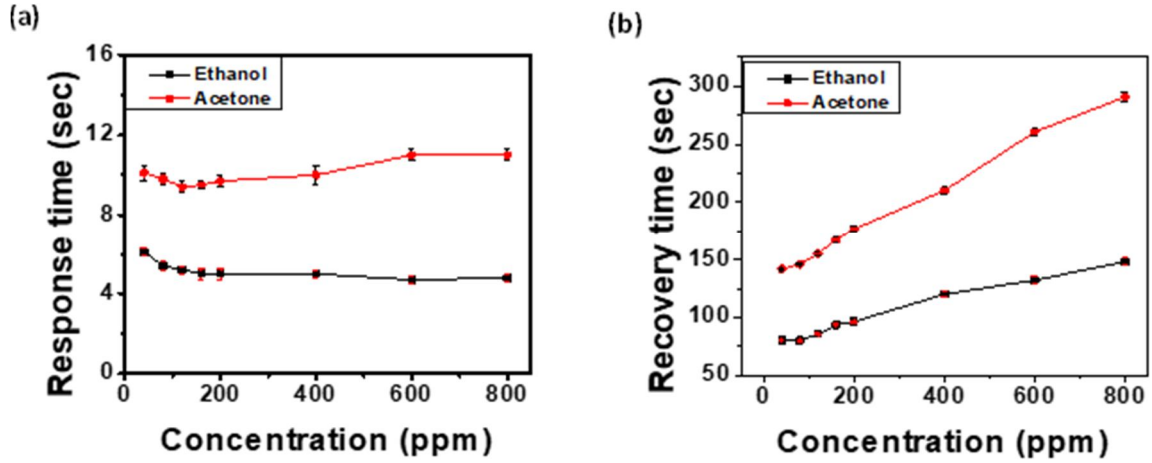

FIG. 9. (a) Response time and (b) recovery time at 40-800 ppm of ethanol and acetone vapor exposure at 285 °C.

TABLE 1. Comparison of the ethanol-sensing result of this work with the published reports

Materials	Method	Operating Temperature (°C)	Ethanol (ppm)	Response or Sensitivity (%)	Res/Rec time (sec)	References
ZnO nanofibers	Electrospining	300	1000	46.4	3/8	[17]
NiO/ZnO	Solvothermal	400	800	40	2.1/4.1	[18]
Al-ZnO	Thermal evaporation	290	3000	200	8/10	[22]
ZnO	Thermal evaporation	250	450 50	22 4.2	NR	[28]
Fe-ZnO	RF Magnetron sputtering	300	300	2.91	20/38	[39]
Fe-ZnO	Hydrothermal	270	500	19		[42]
ZnO	Co-precipitation	285	800 40	52.08 ± 1.23 4.06 ± 0.49	4.8/148 5.4 /180	This work

$$\text{Response} = \frac{R_a}{R_g} \text{ and sensitivity} = \frac{R_a - R_g}{R_a} \times 100\%$$

TABLE 2. Comparison of the acetone-sensing result of this work with the published reports

Materials	Method	Operating Temperature (°C)	Acetone (ppm)	Response or Sensitivity (%)	Res/Rec time (sec)	References
ZnO Sn-ZnO	Vapor-Solid Technique	370	200	65% 90%	NR	[15]
NiO/ZnO	Solvothermal	400	500	Nearly 5	NR	[18]
Sb-In_2O_3	Spray Pyrolysis	300	80	Nearly 95%	NR	[20]
ZnO	Fecile Solution	300	3000	170	1.5/3	[21]
La-ZnO	Solvothermal	425	1000	1826	16/3	[27]
ZnO	Sol-gel	340	500	63		[30]
ZnOnps Pd-ZnOnps	Chemical Solution	370 340	100 100	36 76	12/14 8/10	[32]
ZnOnps	Co-precipitation	285	800 40	25.61±1.21 3.49 ± 0.58	11/291 10.1 /141	This work

4. Conclusions

To sum up, the 0.5M ZnO NPs powder prepared by the co-precipitation method exhibited a polycrystalline nature with a mean crystallite size of 27.39 ± 0.55 nm. The morphological and elemental analyses revealed a flake-like structure with a high degree of purity. The ZnO film showed a better response to ethanol than to acetone. The gas response value at 800 ppm ethanol exposure at 285 °C was nearly twice that of acetone at the same concentration, with values of 53.5284 ± 1.2311 and 25.6119 ± 1.2111 for 800 ppm ethanol and acetone exposure, respectively. Also, the film exhibited faster response and recovery times when tested with ethanol compared to acetone. The response time and recovery time were 5 ± 1 s and 148 ± 3 s, respectively, at 800 ppm ethanol exposure and 11 ± 1 s and 290 ± 4 s for the same concentration of acetone exposure at 285 °C. Upon comparison with the published reports, the outcomes of this work were determined to be efficacious. The gas response towards ethanol was found to be greater than that reported in earlier literature. Remarkably, this work concludes that the 0.5M ZnO film can be useful to fabricate a stable, inexpensive gas sensor that can effectively detect extremely low concentrations (40 ppm) of ethanol and acetone vapors, which is somewhat below the OSHA-recommended lower limit of health hazards.

Data Availability

Data will be provided upon request.

Conflict of Interest

The authors declare that there are no known financial or personal conflicts that could have influenced the conclusions of this work.

Funding statement

This work was partially supported by the Institute of Science and Technology at Tribhuvan University, Nepal, which provided funding for the fabrication of the gas sensor setup and the procurement of necessary chemicals.

Acknowledgements

The authors are thankful to the Indian Institute of Technology (IIT) in Roorkee, Uttarakhand, India, for carrying out the SEM and EDX experiments.

References

[1] Xavier, J.R., Dhanalakshmi, C., Chandraraj, S.S., and Vinodhini, S.P., Trans. Nonferrous Met. Soc. China, 33 (2023) 2136.

[2] Kidowaki, H., Oku, T., Akiyama, T., Suzuki, A., Jeyadevan, B., and Cuya, J., J. Mater. Sci. Res., 1 (2011) 138.

[3] Liu, Q., Wang, B., Wang, Z., Wang, B., Xie, F., and Chang, J., Mater. Today: ProcA2333, 2S (2015) S348.

[4] Sabir, S., Arshad, M., and Chaudhari, S.K., Sci. World. J., 2014 (2014) 1.

[5] Roy, S. and Basu, S., Bull. Mater. Sci., 25 (2002) 513.

[6] Zahoor, R., Jalil, A., Ilyas, S.Z., Ahmed, S., and Hassan, A., Result Surf. Interfaces, 2 (2021) 100003.

[7] Mohd Adnan, M.A., Julkapli, N.M., and Abd Hamid, S.B., Rev. Inorg. Chem., 36 (2016) 77.

[8] Cui, J., Shi, L., Xie, T., Wang, D., and Lin, Y., Sens. Actuators B Chem., 227 (2016) 220.

[9] Zhu, L. and Zeng, W., Sens. Actuators A Phys., 267 (2017) 242.

[10] Wei, A., Pan, L., and Huang, W., J. Mater. Sci. Eng. B, 176 (2011) 1409.

[11] Luo, Y., Ly, A., Lahem, D., Zhang, C., and Debliquy, M., J. Mater. Sci., 56 (2021) 3230.

[12] Poloju, M., Jayababu, N., Ramana Reddy, M.V., J. Mater. Sci. Eng. B., 227 (2018) 61.

[13] Do, J.-S. and Wang, S.-H., Sens. Actuators B Chem., 185 (2013) 39.

[14] Cai, Y., Fan, H., Xu, M., Li, Q., and Long, C., Cryst. Eng. Comm., 15 (36) (2013) 7339.

[15] Sinha, S.K. and Ghosh, S., Adv. Powder Technol., 28 (2017) 2766.

[16] Liu, B. and Zeng, H.C., J. Am. Chem. Soc., 125 (2003) 4430.

[17] Wang, W., Huang, H., Li, Z., Zhang, H., Wang, Y., Zheng, W., and Wang, C., J. Am. Ceram. Soc., 91 (2008) 3817.

[18] Deng, X., Zhang, L., Guo, J., Chen, Q., Ma, J., Mater. Res. Bull., 90 (2017) 170.

[19] Bamsaoud, S.F., Rane, S.B., Karekar, R.N., and Aiyer, R.C., Sens. Actuators B Chem., 153(2) (2011) 382.

[20] Pramod, N.G. and Pandey, S.N., Ceram. Int., 40 (2014) 3461.

[21] Qi, Q., Zhang, T., Liu, L., Zheng, X., Yu, Q., Zeng, Y., and Yang, H., Sens. Actuators B Chem., 134 (1) (2008) 166.

[22] Yang, Z., Huang, Y., Chen, G., Guo, Z., Cheng, S., and Huang, S., Sens. Actuators B Chem., 140 (2) (2009) 549.

[23] Arshak, K. and Gaidan, I., Mater. Sci. Eng. B, 118 (2005) 44.

[24] Lei, M., Gao, M., Yang, X., Zou, Y., Alghamdi, A., Ren, Y., Deng, Y., and ACS, Y., Appl. Mater. Interfaces, 13 (44) (2021), 51933.

[25] Harper, C. and Matsumoto, I., Curr. Opin. Pharmacol., 5 (2005) 73.

[26] Tang, H., Li, Y., Zheng, C., Ye, J., Hou, X., and Lv, Y., Talanta 72 (2007) 1593.

[27] Chu, X., Zhu, X., Dong, Y., Ge, X., Zhang, S., and Sun, W., J. Mater. Sci. Technol., 28 (2012) 200.

[28] Bhatia, S., Verma, N., and Bedi, R.K., Results Phys., 7 (2017) 801.

[29] Yoo, R., Güntner, A.T., Park, Y., Rim, H.J., Lee, H.-S., and Lee, W., Sens. Actuators B Chem., 283 (2019) 107.

[30] Deshwal, M. and Arora, A., J. Mater. Sci. Mater. Electron., 29 (2018) 15315.

[31] Shanthi, S., Subramanian, C., and Ramasamy, P., Mater. Sci. Eng. B, 57 (1999) 127.

[32] Zhang, Y.-H., Liu, C.-Y., Jiu, B.-B., Liu, Y., and Gong, F.-L., Res. Chem. Intermed., 44 (2018) 1569.

[33] Chaudhary, D.K., Kshetri, M.B., Thapa, S., and Joshi, S.K., Mater. Sci. Forum, 1074 (2022) 107.

[34] Srinivasulu, T., Saritha, K., and Reddy, K.T.R., Mod. Electron. Mater., 3 (2017) 76.

[35] Ilican, S., Caglar, Y., and Caglar, M., J. Optoelectron. Adv. Mater., 10 (2008) 2578.

[36] Seiyama, T. and Kagawa, S., Anal. Chem., 38 (1966) 1069.

[37] Roy, T.K., Sanyal, D., Bhowmick, D., and Chakrabarti, A., Mater. Sci. Semicond. Process, 16 (2013) 332.

[38] Kwon, C.H., Hong, H.-K., Yun, D.H., Lee, K., Kim, S.-T., Roh, Y.-H., and Lee, B.-H., Sens. Actuators B Chem., 25 (1995) 610.

[39] Hassan, M.M., Khan, W., Naqvi, A.H., Mishra, P., and Islam, S.S., J. Mater. Sci., 49 (2014) 6248.

[40] Hongsith, N., Wongrat, E., Kerdcharoen, T., and Choopun, S., Sens. Actuators B Chem., 144 (2010) 67.

[41] Kulandaisamy, A.J., Reddy, J.R., Srinivasan, P., Babu, K.J., Mani, G.K., Shankar, P., and Rayappan, J.B.B., J. Alloys Compd., 688 (2016) 422.

[42] Khayatian, A., Kashi, M.A., Azimirad, R., and Safa, S., J. Phys. D Appl. Phys., 47 (2014) 075003.